Schlagermann and Reinicke
Geothermal Energy (2023) 11:33
https://doi.org/10.1186/s40517-023-00276-0

Geothermal Energy

RESEARCH

Open Access

Modeling and economic evaluation of deep geothermal heat supply systems using the example of the Wealden near Hannover, Germany

Pascal Schlagermann[1] and Kurt M. Reinicke[2*]

*Correspondence:
kurt.m.reinicke@tu-clausthal.de

[1] Stadtwerke Düsseldorf AG, Düsseldorf, Germany
[2] Clausthal University of Technology, Clausthal-Zellerfeld, Germany

Abstract

Germany desires to become climate-neutral in its heat supply by 2045. From 2024 onward communities are legally required to develop a plan documenting how the objective will be achieved. Geothermal resources can be a major building block to reach the aspirational target if they can be developed at competitive costs. To evaluate the economic potential of geothermal resources is time and money consuming. Questions which need to be addressed in the context of such evaluations are: how can an economic recovery of geothermal heat be achieved, how can subsurface risks associated with an exploration be managed, and how competitive is a deep geothermal energy recovery compared to other options of heat supply? These questions are key to a development of deep geothermal heat, especially if the geothermal conditions are not as prominent as in already realized projects, but less favorable as in the deep clastic sediments of the North German Basin. With this contribution a procedure is presented and used to determine net present values and the associated levelized costs for deep hydrothermal heat recovery systems. It consists of modelling the geothermal cycle, sizing all necessary components, costing them, and calculating net present value and levelized cost. The thermal model is verified by comparing the modelled state variables pressure and temperature at relevant state points of the thermal cycle with actual data of a geothermal project. The cost model is validated with bidding results and cost information from actual projects and modified as appropriate. In applying the model to a setting in the Hannover–Celle area with temperatures of around 70 °C, conditions are determined, which lead to positive net present values. The degree of their influence is determined in sensitivity analyses allowing a systemic optimization. The results show that for a coupled heat plant with geothermal heat supplied at baseload conditions, levelized costs of approx. 8 cents/kWh are achievable. The presented thermodynamic and cost models are considered helpful instruments for developing preliminary conceptual estimates, strategies for optimization, and portfolio management.

Keywords: Deep geothermal energy, Heat recovery, Wealden Hannover, Economic efficiency, Computer modeling

Introduction

Germany desires to become climate-neutral in its heat supply by 2045. From 2024 onward communities are legally required to develop a plan documenting how the objective will be achieved. Geothermal resources can be a major building block to reach the aspirational target, because the subsurface can both provide and store base-load heat, independent of volatile sources as wind and sun. The question is: are these resources competitive with other sustainable heat sources. The answer requires an evaluation of economics and risks taking local conditions into account.

Many research papers on deep geothermal energy have been published in recent years. They typically address high enthalpy systems. The production process of electrical energy in geothermal power plants is the focus of Sanchez et al. (2013). Cost Estimation models for geothermal power cycle configurations are the subject of (Shamoushaki et al. 2021). Optimal and sustainable geothermal reservoir exploitation is the content of (Blank et al. 2021).

In the literature, a system is known as high enthalpy, when the geothermal fluid has a temperature above 150 °C. At this temperature it may be used to generate electricity. When the geothermal fluid has a temperature between 90 and 150 °C, it is known as a medium enthalpy resource with a typical use for distribution via high temperature district heating networks. Below this temperature, systems are called low enthalpy. They are typically used to provide hot water and space heating, to heat green houses, to enable drying processes, for balneological purposes etc., directly or via medium or low temperature networks. Depending on supply temperature and customer requirements, heat pumps may be necessary to raise the temperature.

While high enthalpy systems have always been in the focus, few publications address the challenges of lower enthalpy systems in an attempt to quantify their thermal power, expected/net present values, EMV/NPV, and levelized costs of heat (Mijnlieff et al. 2012; Wees et al. 2012; ETHZ 2020; NREL 2018), LCOH. This would allow comparisons with other competing assets or other sources of heat supply without investing an appreciable amount of time and money for preliminary investigation, including rough design and bidding process.

This contribution focuses on deriving (pre-tax) net present values for the success case of a geothermal heat plant, and its levelized costs or unit technical costs (Wikipedia 2023):

$$\mathrm{NPV} = \sum_{i=1}^{i=n} \left[\mathrm{Revenue}_i - \left(\mathrm{Capex}_i + \mathrm{Opex}_i\right)\right] \cdot \frac{1}{(1+Z)^i} \tag{1}$$

$$\mathrm{LCOH} = \frac{\text{sum of costs over lifetime}}{\text{sum of heat energy produced over lifetime}} = \frac{\sum_{i=1}^{n} \frac{\mathrm{Capex}_i + \mathrm{Opex}_i}{(1+Z)^i}}{\sum_{i=1}^{n} \frac{\mathrm{Work_i}}{(1+Z)^i}}. \tag{2}$$

Here, Capex and Opex are the capital and operating expenditures, respectively, n is the project lifetime and Z is the discount rate. Together with a probability of success, POS, the net present value may be used to determine an expected monetary value, EMV, according to

$$\mathrm{EMV} = \mathrm{POS} \cdot \mathrm{NPV} - (1 - \mathrm{POS}) \cdot \mathrm{Risik\_capital}. \tag{3}$$

The issue of risk is addressed in companion papers (Reinicke et al. 2022; Hollmann et al. 2023).

For a geothermal system with capacity P_{gt} that is coupled to another heat generation system with capacity P_{coup} to increase its full load hours, FLH_{gt}, the revenue is determined by

$$\mathrm{Revenue} = \left(P_{\mathrm{gt}} \cdot \mathrm{FLH}_{\mathrm{gt}} + P_{\mathrm{coup}} \cdot \mathrm{FLH}_{\mathrm{coup}}\right) \cdot \mathrm{Pr}_{\mathrm{th}} \tag{4}$$

where Pr_{th} is the heat price. The recoverable geothermal power is given by

$$P_{\mathrm{gt}} = \dot{m} \cdot c_p \cdot (T_i - T_o) \tag{5}$$

where $\dot{m}$ is the thermal water mass flow rate, c_p is the isobaric heat capacity, and T_i/T_o is the flow/return temperature.

This work is based on the exergo-economic analyses of Schlagermann for geothermal power plants (Schlagermann 2014) and the associated MATLAB code. For a given mass flow rate from a known reservoir, developed by wells of known design, Schlagermann's work allows the thermodynamic modelling of a deep geothermal recovery process. The relationships used in the model to determine the state variables pressure and temperature are presented. Based on their knowledge the components of the thermal cycle are sized. Models are presented to cost activities, components, and operations. Together with market information, the results are used to determine cash-in and cash-out and carry out net present value and levelized cost calculations, see Fig. 1 for a flow chart of the code to calculate geothermal project economics.

The model is set up to enable a coupling of a geothermal with another heat generation system. This allows investigating thermal systems, utilizing geothermal energy as base load with high full load hours.

The MATLAB code coupled to Refprop has a modular structure allowing a quick adjustment to changing technical or monetary conditions or even to conceptual changes like the use of the geothermal resource for heat recovery and seasonal storage or the inclusion of large heat pumps etc.

The model is applied to evaluate a geothermal heat supply from aquifers in clastic sediments at 1200 to 1400 m depth in the Hannover–Celle area. With an aquifer temperature of 75 °C the resource is low enthalpy, albeit able to feed directly into a district heating network.

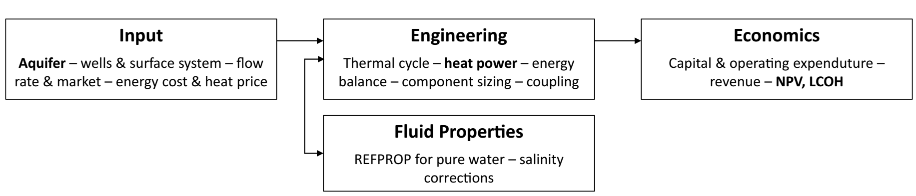

Fig. 1 Flow chart for calculating geothermal project economics

For a systemic optimization, the influences of the most important parameters on the economic indicators are presented. Investigated parameters are heating price, thermal water mass flow rate, geothermal full load hours, thermal water return temperature, electricity purchase price, and financial support.

Methodology

A geothermal cogeneration plant mainly consists of a thermal water-bearing reservoir, wells for its development, and the surface plant components of the thermal water system, heat extraction and/or power generation plant (Schlagermann 2014). The thermal water is pumped to the surface by a suitable pumping device and returned to the reservoir after transferring its heat. A schematic layout of a geothermal heat plant for direct heat supply is shown in Fig. 2. For layouts of geothermal power and cogeneration plants, the reader is referred to Schlagermann (2014).

The focus of this study is a geothermal heat plant used to provide base load heat, coupled with another system for peak load supply. To evaluate its present value and levelized cost, the heat power is quantified by thermodynamic modelling and—together with market information—used to generate the annual cash-in. Modelling results are also used to size the necessary components of the heat cycle and to estimate their capital and operating expenditures by parametric cost models to generate cash-out.

Modeling the thermal cycle and prognosis of thermal power

Quantification of the surface heat recovery requires modeling the water cycle from the reservoir to the surface and back. For its execution, the reference or state points (ZP) shown in Fig. 2a are distinguished (Schlagermann 2014). To quantify the changes of the state variables pressure and temperature between these points, the processes shown in Fig. 2b

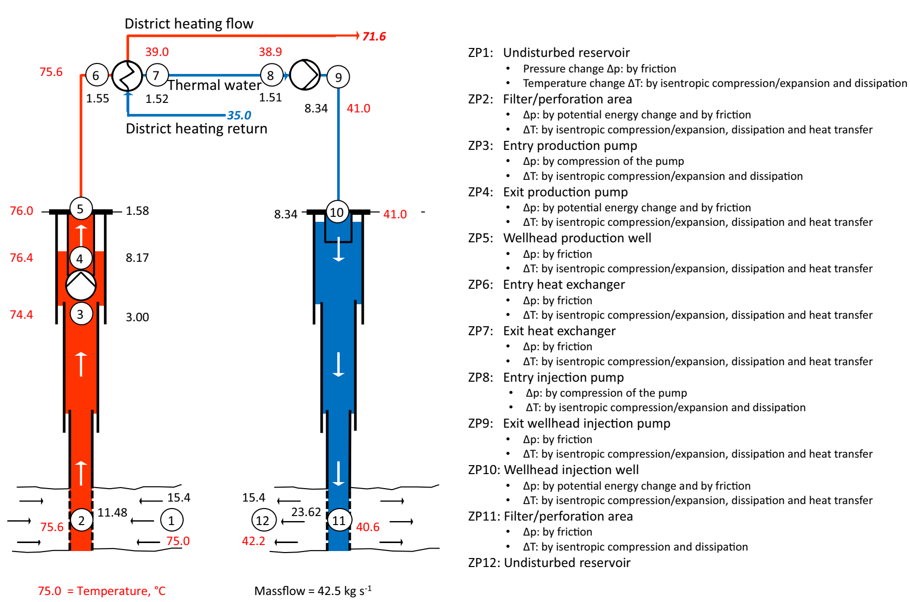

Fig. 2 **a** Schematic diagram of a geothermal heating plant. **b** Considered processes for the thermodynamic description of the thermal water cycle

were considered, which represents the workflow for the thermodynamic calculations. The respective relations to carry out the calculations are detailed in Table 1.

Starting from the undisturbed reservoir at ZP1, the state variables of the thermal water system are determined up to the inlet of the injection pump at ZP8. The *pressure at* ZP2 is calculated by superpositioning the results of the unsteady state well equation for production and injection, equation for $p(r,t)$ in Table 1. The pressure distribution after 6 months of operation around ZP2 and ZP11 for the doublet, described in more detail later, see Table 6, is shown in Fig. 3. Production funnel and injection cone were calculated with densities and viscosities based on the undisturbed reservoir temperature and based on the return temperature into the reservoir, respectively. The higher pressure-buildup around the injection well compared to the drawdown around the production well is due to the higher viscosity of the return flow. It can be assumed that the difference between drawdown and buildup is overestimated with the chosen approach, since the heating of the cooled water in the reservoir is not modeled. The influence of dissolved gases on viscosity is also not considered. These are the subject of further investigations.

The *temperature at* ZP2 is obtained by superpositioning a temperature change due to isentropic expansion and friction-induced dissipation, see Table 1. Thermal water properties are determined using the software Refprop (Lemmon et al. 2018) for pure water and the semi-empirical model of Pitzer et al. (1984) for density, enthalpy, and entropy, and Shide and Zhenhao (2008) for viscosity, and an empirical model of Ozbek and Phillips (1980) for thermal conductivity to correct for salinity.

From ZP2, the fluid flows vertically upward in the casing to enter the production pump at ZP3. From the pump exit it rises in the tubing string to the wellhead at ZP5. In the process, potential energy changes, frictional losses, expansions, and thermal losses to the rock and in the tubing to the annulus occur. These processes are each calculated for borehole sections of different geometry. To minimize errors, the calculation is iterative and discretization is performed as appropriate. The longitudinal heat conduction is neglected. The law of conservation of energy is used to quantify the error with the requirement to not exceed 2% at each state point.

The pressure changes in the borehole and in the production tubing are determined for steady-state conditions due to changes of potential energy of the mineralized thermal water and due to friction using the Darcy or Fanning equation as described by Beggs and Brill (1973), and Beitz and Grote (2001), see Table 1. For the determination of the pipe friction coefficient, a distinction is made between laminar and turbulent flow, and hydraulically smooth and rough pipes. For the non-laminar conditions prevailing in the small diameter well piping of geothermal wells at high rates the friction coefficient λ can be approximated by (Zanke 1993; Bohl and Elmendorf 2005)

$$\lambda = \left\{ -0.868 \cdot \ln\left[\frac{1}{3.71} \cdot \frac{\varepsilon}{d} + \frac{(\ln \mathrm{Re})^{1.2}}{\mathrm{Re}} \right] \right\}^{-2} \quad \text{for } 65 < \mathrm{Re} \cdot \frac{\varepsilon}{d} < 1300 \tag{6}$$

and

$$\lambda = 0.0055 + 0.15 \cdot \left(\frac{\varepsilon}{d} \right)^{1/3} \quad \text{for } 1300 < \mathrm{Re} \cdot \frac{\varepsilon}{d} \tag{7}$$

Table 1 Thermodynamic model for the thermal water cycle

ZP1 → ZP2 (well inflow)	Δp	Friction: $p(r,t)-p_i=-\frac{\dot{m}\cdot g}{4\cdot\pi\cdot T_{\mathrm{GW}}}\cdot\left(-0,577216-\ln(u)+u-\frac{u^2}{2\cdot 2!}+\frac{u^3}{3\cdot 3!}-\frac{u^4}{4\cdot 4!}+\ldots\right)\cdot 10^{-6}$ with $T_{\mathrm{GW}}=\frac{\rho\cdot g}{\mu}\cdot \mathrm{k}\cdot \mathrm{h}$ *and* $u=\frac{r^2\cdot S}{4\cdot T_{\mathrm{GW}}\cdot t}=\frac{\mu\cdot r^2}{4\cdot k\cdot t}\cdot c\cdot\varphi$
	ΔT	Isentropic expansion: iterative determination on Δp using Refprop plus salinity correction Dissipation $T_{\mathrm{ZP1}}-T_{\mathrm{ZP2}}=\frac{(h_{\mathrm{ZP1}}-h^*_{\mathrm{ZP2}})}{c_{pm}{}^*}$ with $h^*_{\mathrm{ZP2}}=h(p_{\mathrm{ZP2}},T_{\mathrm{ZP1}})$ and $c^*_{pm}=c_p(\frac{p_{\mathrm{ZP2}}+p_{\mathrm{ZP1}}}{2},T_{\mathrm{ZP1}})$
ZP2 → ZP3 (rise to pump)	Δp	Potential change and friction: $\Delta p=\Delta p_{\mathrm{pot}}+\Delta p_{\mathrm{fric}}=\left(L\cdot g\cdot\rho_f+\frac{\lambda\cdot L}{d}\cdot\frac{\rho_f\cdot v^2}{2}\right)\cdot 10^{-6}$
	ΔT	Isentropic expansion: iterative determination on Δp using Refprop plus salinity correction Dissipation: $T_{\mathrm{ZP2}}-T_{\mathrm{ZP3}}=\frac{(h_{\mathrm{ZP2}}-h^*_{\mathrm{ZP3}})}{c_{pm}{}^*}$ *with* $h^*_{\mathrm{ZP3}}=h(p_{ZP3},T_{ZP2})$ and $c^*_{\mathrm{pm}}=c_p(\frac{p_{\mathrm{ZP3}}+p_{\mathrm{ZP2}}}{2},T_{\mathrm{ZP2}})$ Heat losses into the formation: $T_e=T_0+(T_i-T_0)\cdot e^{\left(\frac{-k\cdot U\cdot z}{\rho\cdot v\cdot A\cdot c_p}\right)}$, A = area perpendicular to flow with $k=\frac{1}{R\cdot A}$, $R=\frac{1}{2\cdot\pi\cdot L}\cdot\left(\frac{1}{\alpha_{\mathrm{Brine}}\cdot r_1}+\frac{ln(r_2/r_1)}{\lambda_{\mathrm{Casing}}}+\frac{ln(r_3/r_2)}{\lambda_{\mathrm{Cement}}}+\frac{ln(r_4/r_3)}{\lambda_{\mathrm{Formation}}}\right)$, and $\alpha_{\mathrm{Brine}}=\frac{Nu\cdot\lambda_{\mathrm{Brine}}}{2\cdot r}$
ZP3 → ZP4 (pump)	Δp	Production pump pressure increase: iterative determination to match the surface system pressure
	ΔT	Pump compression: $T_{\mathrm{ZP4,compr}}-T_{\mathrm{ZP3}}=\frac{(h_{\mathrm{ZP4}}-h_{\mathrm{ZP3}})}{c_{\mathrm{pm}}}=\frac{(h_{\mathrm{ZP4,}isentrop}-h_{\mathrm{ZP3}})/\eta_{isentrop}}{c_{\mathrm{pm}}}$ with $c_{\mathrm{pm}}=\frac{c_p(p_{\mathrm{ZP4}},T_{\mathrm{isentrop}})+c_p(p_{\mathrm{ZP3}},T_{\mathrm{ZP3}})}{2}$ Pump motor cooling: $T_{\mathrm{ZP4}}-T_{\mathrm{ZP4,compr}}=\frac{P_{\mathrm{hydr}}\cdot(1-\eta_{\mathrm{Motor}})}{\dot{m}\cdot c_p}$ with $P_{\mathrm{Hydr}}=\dot{V}\cdot\Delta p\cdot 10^{-3}$ and $\dot{V}=\frac{\dot{m}}{(\rho_{\mathrm{ZP3}}+\rho_{\mathrm{ZP4}})/2}$
ZP4 → ZP5 (rise to surface)	Δp	Potential change and friction: $\Delta p=\Delta p_{\mathrm{pot}}+\Delta p_{\mathrm{fric}}=\left(L\cdot g\cdot\rho_f+\frac{\lambda\cdot L}{d}\cdot\frac{\rho_f\cdot v^2}{2}\right)\cdot 10^{-6}$
	ΔT	Isentropic expansion: iterative determination on Δp using Refprop plus salinity correction Dissipation: $T_{\mathrm{ZP4}}-T_{\mathrm{ZP5}}=\frac{(h_{\mathrm{ZP4}}-h^*_{\mathrm{ZP5}})}{c_{\mathrm{pm}}{}^*}$ with $h^*_{\mathrm{ZP5}}=h(p_{\mathrm{ZP5}},T_{ZP4})$ and $c^*_{\mathrm{pm}}=c_p(\frac{p_{\mathrm{ZP5}}+p_{\mathrm{ZP4}}}{2},T_{\mathrm{ZP4}})$ Heat losses to the (gas filled) annulus: $T_e=T_0+(T_i-T_0)\cdot e^{\left(\frac{-k\cdot U\cdot z}{\rho\cdot v\cdot A\cdot c_p}\right)}$ with $k=\frac{1}{R\cdot A}$ and $R=\frac{1}{2\cdot\pi\cdot L}\cdot\left(\frac{1}{\alpha_{\mathrm{Brine}}\cdot r_1}+\frac{ln(r_2/r_1)}{\lambda_{\mathrm{Pipe}}}+\frac{ln(r_3/r_2)}{\lambda_{\mathrm{Annulus}}}\right)$, and $\alpha_{\mathrm{Brine}}=\frac{Nu\cdot\lambda_{\mathrm{Brine}}}{2\cdot r}$
ZP5 → ZP6 (flow to heat exchanger)	Δp	Friction: $\Delta p_{\mathrm{fric}}=\left(\frac{\lambda\cdot L}{d}\cdot\frac{\rho_f\cdot v^2}{2}\right)\cdot 10^{-6}$
	ΔT	Isentropic expansion: iterative determination on Δp using Refprop plus salinity correction Dissipation: $T_{\mathrm{ZP5}}-T_{\mathrm{ZP6}}=\frac{(h_{\mathrm{ZP5}}-h^*_{\mathrm{ZP6}})}{c_{\mathrm{pm}}{}^*}$ with $h^*_{\mathrm{ZP6}}=h(p_{\mathrm{ZP6}},T_{\mathrm{ZP5}})$ and $c^*_{\mathrm{pm}}=c_p(\frac{p_{\mathrm{ZP6}}+p_{\mathrm{ZP5}}}{2},T_{\mathrm{ZP5}})$ Heat losses to the environment: $T_e=T_0+(T_i-T_0)\cdot e^{\left(\frac{-k\cdot U\cdot z}{\rho\cdot v\cdot A\cdot c_p}\right)}$ with $k=\frac{1}{R\cdot A}$ and $R=\frac{1}{2\cdot\pi\cdot L}\cdot\left(\frac{1}{\alpha_{\mathrm{Brine}}\cdot r_1}+\frac{ln(r_2/r_1)}{\lambda_{\mathrm{Pipe}}}+\frac{ln(r_3/r_2)}{\lambda_{\mathrm{Insulation}}}\right)$, and $\alpha_{\mathrm{Brine}}=\frac{\mathrm{Nu}\cdot\lambda_{\mathrm{Brine}}}{2\cdot r}$
ZP6 → ZP7 (heat exchanger)	Δp	2% (input value)
	ΔT	Isentropic expansion: iterative determination on Δp using Refprop plus salinity correction Dissipation: $T_{\mathrm{ZP6}}-T_{\mathrm{ZP7}}=\frac{(h_{\mathrm{ZP6}}-h^*_{\mathrm{ZP7}})}{c_{\mathrm{pm}}{}^*}$ with $h^*_{\mathrm{ZP7}}=h(p_{\mathrm{ZP7}},T_{\mathrm{ZP6}})$ and $c^*_{\mathrm{pm}}=c_p(\frac{p_{\mathrm{ZP7}}+p_{\mathrm{ZP6}}}{2},T_{\mathrm{ZP6}})$ Heat extraction: $P_{\mathrm{gt}}=\dot{m}\cdot c_p\cdot(T_i-T_o)$
ZP7 → ZP8 (flow to Injection pump)	Δp	Friction: $\Delta p_{\mathrm{fric}}=\left(\frac{\lambda\cdot L}{d}\cdot\frac{\rho_f\cdot v^2}{2}\right)\cdot 10^{-6}$
	ΔT	Isentropic expansion: iterative determination on Δp using Refprop plus salinity correction Dissipation: $T_{\mathrm{ZP7}}-T_{\mathrm{ZP8}}=\frac{(h_{\mathrm{ZP7}}-h^*_{\mathrm{ZP8}})}{c_{\mathrm{pm}}{}^*}$ with $h^*_{\mathrm{ZP8}}=h(p_{\mathrm{ZP8}},T_{\mathrm{ZP7}})$ and $c^*_{\mathrm{pm}}=c_p(\frac{p_{\mathrm{ZP8}}+p_{\mathrm{ZP7}}}{2},T_{\mathrm{ZP7}})$ Heat losses to the environment: $T_e=T_0+(T_i-T_0)e^{\left(\frac{-k\cdot U\cdot z}{\rho\cdot v\cdot A\cdot c_p}\right)}$ with $k=\frac{1}{R\cdot A}$ and $R=\frac{1}{2\cdot\pi\cdot L}\cdot\left(\frac{1}{\alpha_{\mathrm{Brine}}\cdot r_1}+\frac{ln(r_2/r_1)}{\lambda_{\mathrm{Pipe}}}+\frac{ln(r_3/r_2)}{\lambda_{\mathrm{Insulation}}}\right)$, and $\alpha_{\mathrm{Brine}}=\frac{\mathrm{Nu}\cdot\lambda_{\mathrm{Brine}}}{2\cdot r}$
ZP8 → ZP9 (Pump)	Δp	Injection pump pressure increase: iterative determination against the direction of flow starting with the undisturbed reservoir pressure
	ΔT	Pump compression: $T_{\mathrm{ZP9}}-T_{\mathrm{ZP8}}=\frac{(h_{\mathrm{ZP9}}-h_{\mathrm{ZP8}})}{c_{\mathrm{pm}}}=\frac{(h_{\mathrm{ZP9,isentrop}}-h_{\mathrm{ZP8}})/\eta_{\mathrm{isentrop}}}{c_{\mathrm{pm}}}$ with $c_{\mathrm{pm}}=\frac{c_p(p_{\mathrm{ZP9}},T_{\mathrm{isentrop}})+c_p(p_{\mathrm{ZP8}},T_{ZP8})}{2}$

Table 1 (continued)

ZP9 → ZP10 (flow to Wellhead)	Δp	Friction: $\Delta p_{\text{fric}} = \left(\frac{\lambda \cdot L}{d} \cdot \frac{\rho_f \cdot v^2}{2}\right) \cdot 10^{-6}$
	ΔT	Isentropic compression: iterative determination on Δp using Refprop plus salinity correction
		Dissipation: $T_{ZP9} - T_{ZP10} = \frac{(h_{ZP9} - h^*_{ZP10})}{c_{pm}{}^*}$ with $h^*_{ZP10} = h(p_{ZP10}, T_{ZP9})$ and $c^*_{pm} = c_p(\frac{p_{ZP10}+p_{ZP9}}{2}, T_{ZP9})$
ZP10 → ZP11 (flow thru casing to reservoir)	Δp	Potential change and friction: $\Delta p = \Delta p_{\text{pot}} + \Delta p_{\text{fric}} = \left(L \cdot g \cdot \rho_f + \frac{\lambda \cdot L}{d} \cdot \frac{\rho_f \cdot v^2}{2}\right) \cdot 10^{-6}$
	ΔT	Isentropic compression: iterative determination on Δp using Refprop plus salinity correction
		Dissipation: $T_{ZP10} - T_{ZP11} = \frac{(h_{ZP10} - h^*_{ZP11})}{c_{pm}{}^*}$ with $h^*_{ZP11} = h(p_{ZP11}, T_{ZP10})$ and $c^*_{pm} = c_p(\frac{p_{ZP11}+p_{ZP10}}{2}, T_{ZP10})$
		Heat losses into the formation: $T_e = T_0 + (T_i - T_0) \cdot e^{\left(\frac{-k \cdot U \cdot z}{\rho \cdot v \cdot A \cdot c_p}\right)}$, A = area perpendicular to flow with $k = \frac{1}{R \cdot A}$, $R = \frac{1}{2 \cdot \pi \cdot L} \cdot \left(\frac{1}{\alpha_{\text{Brine}} \cdot r_1} + \frac{\ln(r_2/r_1)}{\lambda_{\text{Casing}}} + \frac{\ln(r_3/r_2)}{\lambda_{\text{Cement}}} + \frac{\ln(r_4/r_3)}{\lambda_{\text{Formation}}}\right)$, and $\alpha_{\text{Brine}} = \frac{\text{Nu} \cdot \lambda_{\text{Brine}}}{2 \cdot r}$
ZP11 → ZP12 (well outflow)	Δp	Friction: $p(r,t) - p_i = + \frac{\dot{m} \cdot g}{4 \cdot \pi \cdot T_{GW}} \cdot \left(-0,577216 - \ln(u) + u - \frac{u^2}{2 \cdot 2!} + \frac{u^3}{3 \cdot 3!} - \frac{u^4}{4 \cdot 4!} + \ldots\right) \cdot 10^{-6}$ with $T_{GW} = \frac{\rho \cdot g}{\mu} \cdot k \cdot h$ and $u = \frac{r^2 \cdot S}{4 \cdot T_{GW} \cdot t} = \frac{\mu \cdot r^2}{4 \cdot k \cdot t} \cdot c \cdot \varphi$
	ΔT	Isentropic compression: iterative determination on Δp using Refprop plus salinity correction
		Dissipation: $T_{ZP11} - T_{ZP12} = \frac{(h_{ZP11} - h^*_{ZP12})}{c_{pm}{}^*}$ with $h^*_{ZP12} = h(p_{ZP12}, T_{ZP11})$ and $c^*_{pm} = c_p(\frac{p_{ZP12}+p_{ZP11}}{2}, T_{ZP11})$

where Re is the Reynold's number, given by $\text{Re} = \frac{\rho \cdot v \cdot d}{\mu}$.

The temperature changes in the *borehole* due to heat losses into the formation are calculated according to Kalb and Steinhilber (2003) using as model a multilayer hollow cylinder consisting of borehole, and the encasing shells casing, and cement (mantle) embedded in a semi-infinite body for the rock, see Fig. 4. Losses in the tubing are determined for a model consisting of tubing, tubing wall, and (gas filled) annulus with the temperature in the annulus equal to the average undisturbed temperature behind the surface casing, Table 1. The model for the surface piping consists of pipe, pipe wall, and insulation.

The determination of the fluid heat losses requires determining the thermal resistance of the encasing shells, including the transmission of heat from the fluid to the pipe wall, see Table 1. The latter is governed by the convective heat transfer coefficient α_{Brine}. This coefficient is dependent on the flow conditions, introduced by the Nußelt-number, Nu, the thermal conductivity of the fluid, λ_{Brine}, and a characteristic length:

$$\alpha_{\text{Brine}} = \frac{\text{Nu} \cdot \lambda_{\text{Brine}}}{2 \cdot r} \tag{8}$$

and on the fluid properties, represented by the Prandtl number, Pr. For turbulent flow, the Nußelt number is determined according to Wagner (2004), and Beitz and Grote (2001):

$$\text{for } 10^4 < \text{Re} < 10^5 \text{ and } 0.6 < \text{Pr} < 50 \quad \text{Nu} = 0.0235\left(\text{Re}^{0.8} - 230\right) \cdot \text{Pr}^{0.48} \tag{9}$$

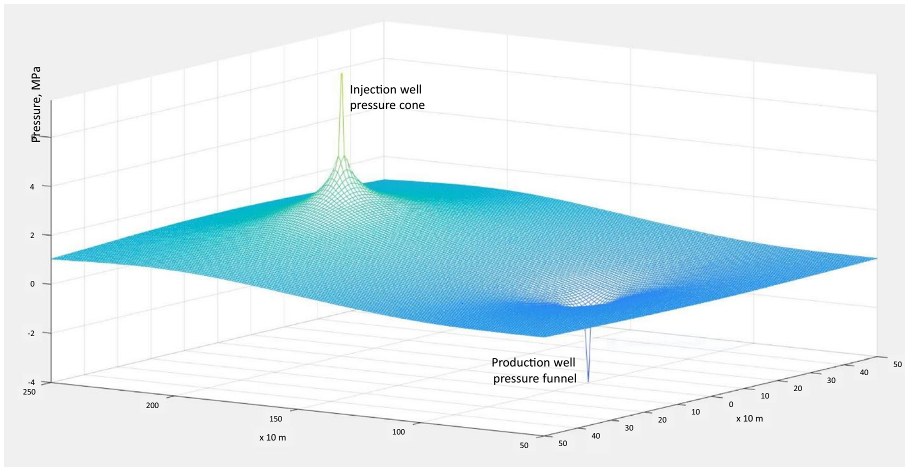

Fig. 3 Reservoir pressure distribution of a doublet (relative to original pressure), 6 months after start of production and injection using the conditions documented in Table 6

$$\text{for } 10^5 < \text{Re} < 10^6 \text{ and } 0.6 < \text{Pr} < 1000 \quad \text{Nu} = \frac{\text{Re} \cdot \text{Pr} \cdot \xi/8}{1 + 12.7 \cdot \sqrt{\xi/8} \cdot \left(\text{Pr}^{2/3} - 1\right)} \left(1 + \left(\frac{2 \cdot r}{l}\right)^{2/3}\right)$$
$$\text{with } \xi = (0.78 \cdot \ln(\text{Re}) - 1.5)^{-2} \tag{10}$$

$$\text{for } 10^6 < Re < 10^7 \text{ and } 0.6 < \text{Pr} < 1000 \quad \text{Nu} = \frac{\text{Re} \cdot \text{Pr} \cdot \xi/8}{1 + 12.7 \cdot \sqrt{\xi/8} \cdot \left(\text{Pr}^{2/3} - 1\right)}.$$
$$\text{with } \xi = (1.8 \cdot \ln(\text{Re}) - 1.5)^{-2} \tag{11}$$

The Prandtl number is given by $\text{Pr} = \frac{\eta \cdot c_p}{\lambda_{\text{Brine}}}$, the Reynold's number is defined as before.

A *pump at* ZP3 suspended from the production tubing delivers the thermal water to the wellhead against the system pressure on the surface. The required system pressure is dependent on the water chemistry and is usually selected above the pressure at which gases in the thermal water dissolve (Herzberger et al. 2009). Setting depth and pressure increase of the production pump are determined iteratively. The criterion

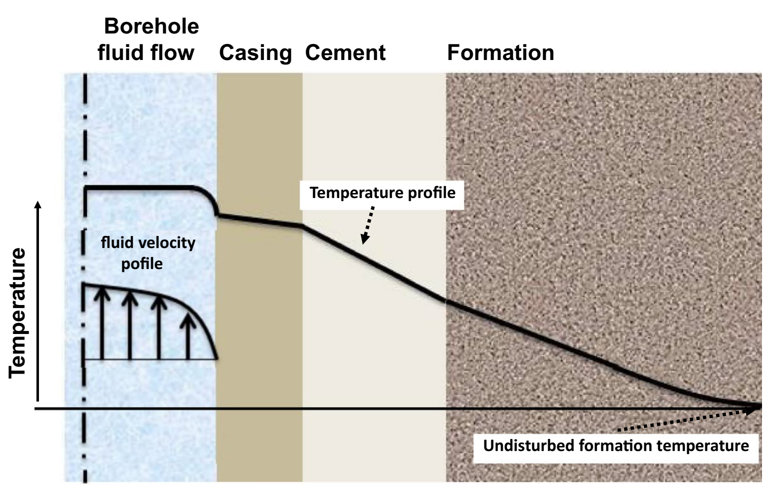

Fig. 4 Heat transfer from a producing well as a special case of a multilayer hollow cylinder

for the setting depth of the pump is a pressure at the top of the fluid column (pump inlet plus minimum submergence) equal to the degassing pressure. Criterion for the pressure increase needed from the pump is a pressure at the wellhead, ZP5, equal to the surface system pressure. The relevant processes between inlet and outlet of the production pump are the pressure increase due to the pump and the temperature increase due to compression in the pump and cooling of the electric motor, see Table 1.

From the *wellhead at* ZP5 of the production well, the thermal water flows through an insulated surface piping to the *heat exchanger at* ZP6, where it transfers its heat to the district heating network. Pressure and temperature losses in the piping are determined as before, Table 1.

After heat extraction the thermal water is reinjected into the reservoir via the wellhead of the injection well, first through an injection string (if any) and then through the casing. Coarse and fine filters upstream of the heat exchanger and the re-injection, respectively, serve to protect the heat exchanger and the reservoir. In addition to these main components, the surface system includes valves and fittings, instrumentation and control equipment, and, depending on specific conditions, for example, dosing equipment for the addition of inhibitors, equipment for gas separation, or for pressure maintenance.

The system is assumed to include a peak-load and redundancy boiler. Contrary to the cost calculation, only the surface piping, heat exchanger, and injection pump are represented in the calculations of the state parameters.

The pressure increase by the *injection pump at* ZP8 results from the back pressure of the reservoir and the flow losses in the injection well. Its determination is made against the direction of flow, starting from the undisturbed reservoir. After an initial estimation of the injection temperature, the pressure losses in the well, and thus the pressure increase due to the injection pump, are determined and then iteratively improved.

A *validation* of the computational model of the thermal water cycle was carried out with data from the Bruchsal geothermal project, see Table 2 (Schlagermann 2014). The measured pressures and temperatures were recorded under quasi steady state conditions. The model predicted and the measured data for pressure and temperature show good agreement at most state points with deviations smaller than approx. 3%. Applying

Table 2 Comparison of measured and calculated pressures for geothermal power plant Bruchsal

	Temperature			**Pressure**		
	Measured	**Calculated**	**Difference**	**Measured**	**Calculated**	**Difference**
	°C	**°C**	**%**	**MPa**	**MPa**	**%**
1: Reservoir	132.8	132.9	− 0.1	25.28	25.28	0.0
2: Wellbore bottom		132.8			21.66	
Production pump	125.9	125.6	0.2	4.45	4.36	2.0
Tubing		126.6			7.09	
Wellhead		126.0		2.16	2.21	− 2.3
6: Heat exchanger in	122.0	125.8	− 3.1	2.09	2.13	− 1.9
6: Heat exchanger in		68.8			2.09	
		–			–	
9: Wellhead	66.8	67.8	− 1.5	2.00	2.00	0.0

the model to the conditions of the Wealden in the Hannover–Celle area, the values of the state variables in Fig. 2a result for the thermal water cycle, if a mass flow of 42.5 kg s^{-1} is assumed, see Table 6.

Error calculations were carried out for each state points on the basis of the law of conservation of energy, yielding values of less than 2%.

A further *validation* was carried out by comparing the calculated results with those of the TNO DoubletCalc v1.4 data set. The results obtained with the 'Geotechnics (Input)' of reference (Mijnlieff et al. 2012) calculated using this code are compared to the 'Geotechnics (Output)' of Mijnlieff et al. (2012) in Table 3.

In general, agreement is good. Differences are caused by the difference in system pressure (input value for this procedure), the degree of detail in the thermodynamic description of the thermal cycle, for example, the consideration of thermal losses in the surface piping, of a pressure loss across the heat exchanger etc. and differences in the PVT property evaluation.

The procedure described here is deterministic. Its extension to include subsurface uncertainties and risks has been presented in Reinicke et al. (2022), Hollmann et al. (2023) using the methodology of Rose (Rose Associates 2007), which is well-established in the oil and gas industry.

Sizing and costing capital expenditures

For sizing and costing, project planning, drilling, production and injection equipment, thermal water system, including heat exchanger, and others are distinguished.

Planning

This phase includes the acquisition and analysis of existing geological, geophysical, and borehole–geophysical information to obtain information about extent, depth, and quality of the geothermal reservoir and identify critical rock formations and geologic fault zones. In areas with little or no information on subsurface temperature, heat flow studies may have to be carried out. If new areal surveys are required, for example, seismic surveys to map the subsurface, or magnetotelluric surveys to obtain indications of geothermally active regions, they are valued depending on the length or

Table 3 Comparison of calculated results with TNO's results

	Temperature			Pressure		
	DoubletCalc	This code	Difference	DoubletCalc	This code	Difference
	°C	°C	%	MPa	MPa	%
Reservoir	89.28	89.2	− 0.1	255.1	255.1	0.0
Wellbore bottom	89.28	89.3	0.0	241.3	246.1	2.0
Wellhead	86.51	85.6	− 1.1	16.35	16.8	2.7
Heat exchanger in	86.51	85.2	− 1.5	16.35	16.5	0.9
Heat exchanger out	35	35	0.0	16.35	16.1	− 1.6
Wellhead	35	35	0.0	16.35	17.7	7.6
Wellbore bottom	35.99	36.8	2.2	277	283.2	2.2
Reservoir	89.28	89.3	0.0	252.2	255.1	1.1

Table 4 Cost model for capital expenditure

Project phase	Project element	Cost model	Time to replacement
Planning	Feasibility study, €	180,000	
	acquisition and analysis of existing information, €	500,000	
	Energy concept, €	100,000	
	Permits, expert opinions, €	150,000	
Drilling	Site, construction reconditioning, €	300,000	Lifetime
	Rigup, €	250,000	
	Drilling expenditure, €	$1.198 \cdot e^{0.0004354 \cdot z_{MD}} \cdot V_{\mathrm{Well}}/V_{\mathrm{Ref.Well}} \cdot 10^6$	
	Logging, €/m	65	
	Production/circulation test, €	450,000/350,000	
	Stimulation, €	600,000	
Production and injection equipment	Production pump, €	$P_{\mathrm{Hydr}} \cdot \left(M \cdot P_{\mathrm{Hydr}}^{-0.319}\right)$, where $P_{\mathrm{Hydr}} = \mathrm{NPF} \cdot \dot{V} \cdot \Delta p$	4
	Pump Installation, €	$5000\left[euro/\mathrm{d}\right] \cdot \left(\frac{\mathrm{Setting\_depth[m]}}{250[\mathrm{m/d}]} + 4\right) + 10{,}000[euro]$	
	Completion excl. pump, €	$L[\mathrm{m}] \cdot \left\{80 + \left(0.0215 \cdot P_{\mathrm{Hydr}} + 77\right)\right\}$	
	Injection pump, €	$0.8 \cdot \left[1500 \cdot {P_{\mathrm{Cap\_inj}}}^{0.48}\left(1.89 + 1.35 \cdot \mathrm{FM} \cdot 10^{\left(-0.3935+0.3957 \cdot \log_{10}(p)-0.00226 \cdot \log_{10}(p)^2\right)}\right)\right]$, where $P_{\mathrm{Cap\_inj}} = \mathrm{NPF} \cdot \dot{V} \cdot \frac{\Delta p}{\eta_{\mathrm{Motor}} \cdot \eta_{\mathrm{Isentropic}}}$ and p = operating pressure in barue	10
Thermal water system incl. heat exchanger	Surface piping incl. fittings, €/m	$\mathrm{Capex}_{\mathrm{Pipe\_}p_{15}}\left[euro/\mathrm{m}\right] = M1 \cdot \dot{V}\left[\mathrm{m}^3/\mathrm{s}\right] + M2$ $\mathrm{Capex}_{\mathrm{Pipe}}\left[euro/\mathrm{m}\right] = \mathrm{Capex}_{\mathrm{Pipe\_}p_{15}} \cdot \left[1 + \alpha \cdot (p - p_{15})\right]$	Lifetime
	Pressure vessel, €	$\mathrm{Capex}_{p_{15}} = 10^{\left(3.4974+0.4485 \cdot \log_{10}(V)+0.1074 \cdot \log_{10}(V)^2\right)}$ $\mathrm{Capex} = \mathrm{Capex}_{15} \cdot [2.25 + 1.82 \cdot \mathrm{FM} \cdot \mathrm{FP}]$ $\mathrm{FP} = \left(\frac{p \cdot d}{2 \cdot (850-0.6 \cdot p)} + 0.00315\right)/0.0063$ with p = operating pressure in barue	Lifetime
	Shell-and-tube heat exchanger, €	$1300 \cdot A^{0.66} \cdot \left(1.63 + 1.66 \cdot FM \cdot 10^{\left(0.03881-0.11272 \cdot log_{10}(p)+0.08183 \cdot log_{10}(p)^2\right)}\right)$ with $A\left[\mathrm{m}^2\right] = \frac{P_{\mathrm{th}}}{\dot{q}_W \cdot \Delta T_{\log}} \cdot \mathrm{NPF}$ and $\Delta T_{\log}[K] = \frac{\Delta T_{\max}-\Delta T_{\min}}{\ln \frac{\Delta T_{\max}}{\Delta T_{\min}}}$	10
	Peak load and redundancy boiler, €	$\mathrm{FM} \cdot 1150 \cdot \left(\mathrm{NPF} \cdot P_{\mathrm{gt}}/\mathrm{Share}_{\mathrm{gt}}\right)^{0.56}$	20
Other capital expenditure	Project management	8% of Capex for drilling/surface facilities	
	Insurance	3.5/0.5% of Capex for drilling/surface facilities	
	Seismic monitoring, €	150,000	
	Public relations, €	400,000	

M, FM = Material factor; α, FP = Pressure factor; NPF = Name plate factor, for values see text

the area of the surveys, taking into account the respective environmental conditions. The costs incurred in acquiring new information, which is not included, may be substantial. The expenditures for all other efforts are estimated by lump sum values per project, Table 4.

Drilling

The construction costs of the necessary wells are determined by the number of well sites and the drilling expenditures. For the well sites, an area of 2400 m^2 per site is assumed (Fromme 2005). Drilling expenditures are estimated on the basis of well depth and wellbore diameter. To account for wellbore deviations and different wellbore diameters, the approach of Guth (2011) for vertical wells is modified. The vertical depth is replaced by the actual length of the borehole, and the actual borehole volume is set in relation to a reference volume (Schlagermann 2014) defined for a borehole with three or four sections of different diameters (Sperber et al. 2008).

Production and injection equipment

The capital expenditures of the production equipment consist of the power-dependent expenditures for the subsurface pump, the depth-dependent expenditures for production tubing and power cable, and the time-dependent expenditures for installation/removal.

Production pump expenditures are determined as in Table 4 with $M = 11{,}685$ for a standard version and $M = 14{,}145$ for a stainless-steel version and a Name Plate Factor $NPF = 1.15$ to correct the hydraulic (operating) power to design power. An additional allowance factor of 1.1 accounts for coordination, supervision, and possible provision of power, water, and lifting equipment by the contractor.

The expenditures for the tubing and power cable are determined depending on length as in Table 4. The costs for pump installation and removal are determined depending on time, assuming an installation speed of 250 m/day. For mobilization and demobilization, €10,000 plus 1 day rate each is assumed. An additional day is estimated for pump installation and waiting time. The per diem for personnel and machinery is assumed to be 5000 €/d.

The capital expenditure for a possibly necessary injection pump is calculated with a modified equation according to Turton et al. (2009) for centrifugal pumps. As operating pressure p, the outlet pressure in barue is used. A Name Plate Factor of 1.1 provides a 10% reserve. A material factor of 2.3 reflects a stainless-steel version. The factor 0.8 is added to account for systematically too high estimates of capital expenditure.

Thermal water system incl. heat exchanger

These capital expenditures consist in particular of the surface piping, the fittings, the heat exchanger, the filters, any pressure vessels, the peak load and redundancy boiler, and the instrumentation and control equipment.

Capital expenditures for surface piping and pressure vessels are first determined for a reference pressure and then adjusted to the actual pressures, Table 4. The subscript in p_{15} denotes a reference pressure of 15 barue.

To cost the surface piping at 15 barue reference pressure, values of 55,000 and 1150 are used for the factors $M1$ and $M2$ in case of the thermal water system, and 3000 and 400 for the connecting flowline in case of two well sites. The lower values in the flowline case reflect the fact that fewer valves and I&C are installed. For the factor α in the pressure scaling relation, 0.03 is used for the thermal water system and 0.02 for the site-connecting line.

The expenditures for filters and other pressure vessels are calculated according to Turton et al. (2009) for upright standing vessels without internals. Two redundant filters are provided upstream of the heat exchanger and two more downstream. The vessel volume, V, is calculated from the thermal water flow rate and a maximum flow velocity of 0.15 m s^{-1}. The component costs are calculated for reference conditions.

The design of the heat exchanger is assumed to be of shell-and-tube type. The heat exchanger area is calculated assuming a heat flux density, $\dot{q}_W$, typical for a district heat extraction, together with a name plate factor of 1.2. The relationship in Table 4 is applicable for operating pressures greater than 0.5 MPa. As operating pressures p in barue, 1.2 times the system operating pressure is assumed. A material factor of 1.81 reflects a carbon steel/stainless steel design.

The peak load boiler is sized to provide redundancy for the total system heat power given by $P_{\mathrm{gt}}/\mathrm{Share}_{\mathrm{gt}}$, Table 4. A material factor of 4 and a Name Plate Factor of 1.0 is used to calculate the boiler expenditure.

Other capital expenditures

Considered expenditures are listed in Table 4.

Operating expenditures

For operating expenditures energy/resources-related costs, operation-related costs and other costs are distinguished in line with the recommendations of the VDI 2067 (VDI 2010).

Energy/resources-related costs

They are dominated by the electricity demand for the production and the injection pump, and in case of a coupling with a peak heat generator, with its consumption costs.

The electricity cost for the production pump is derived from the pump capacity, the energy cost for the peak heat generator from its supply capacity. Both calculations take into account the respective efficiencies and the full load hours, see Table 5. The energy-related cost of the injection pump is determined similarly.

In addition to the cost of operating the pumps and the coupled heat generator, there are costs for other operating supplies, such as costs for working fluids, disposal costs, inhibitors, fresh/wastewater, and other power consumptions.

Operation costs

They consist of personnel costs and maintenance and repair costs. Personnel costs consist of costs associated with operations, administration and other personnel expenses, remote monitoring, and seismic monitoring operations.

For *Other costs,* see Table 5.

Case study Wealden in the Hannover–Celle area

The methodology is applied to evaluate a potential project in the Hannover–Celle area. There, several sandstone layers are encountered in the Wealden formation at a depth of about 1200 to 1400 m. Due to an anomaly [likely due to a temperature "dog leg" caused by formations of low heat conductivity above the Wealden, resulting in heat

Table 5 Cost model for operating expenditure per year

Energy/resource-related	Energy, €	$\mathrm{Pr}_{el} \cdot \frac{P_{hydr}}{\eta_{motor} \cdot \eta_{isentrop} \cdot \eta_{FU}} \cdot \mathrm{FLH}_{gt}$
	Other operating supplies, e.g., working fluids, disposal costs, inhibitors, fresh/wastewater, and other power consumptions, €	1% of capital expenditures for the relevant items
Operations-related	Own personnel, €	$220,000 \cdot e^{5 \cdot 10^{-6} \cdot P_{th}[\mathrm{kW}]}$
	Remote monitoring and standby service, €	25% of own personnel cost
	Seismic monitoring, €	60,000
	Maintenance and repair wells, €	0.5% of well cost
	Maintenance and repair surface facilities, €	3% of capital expenditures for surface facilities
Other	Liability insurance costs, €	90,000
	Insurance for electronic and machinery breakdown, €	0.6% of capital expenditure
	Administrative costs not yet taken into account (e.g., legal counsel) and public relations, €	25,000

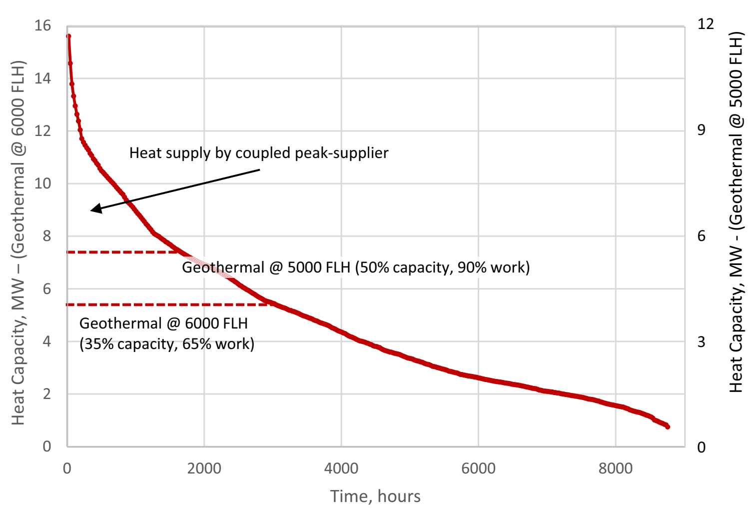

Fig. 5 Heat load profile

to accumulate and thus higher thermal gradients (Walzebuck and Gaupp 1991)], the thermal water of the sands has a temperature of about 75 degrees Celsius at a depth of 1300 m. For the water, a similar composition is assumed as in the Hannover well Gross-Buchholz Gt1 (Tischner and Krug 2010).

For the market, the heat demand and load structure of a small town with an annual load profile as shown in Fig. 5 is assumed. The portrayed load structure represents the mean of the Umwelt–Bundesamt load structure for a model small town (Umweltbundesamt 2018) and own surveys in the area. Figure 5 also shows splits in serving this demand by a geothermal resource, with and without coupling to serve peak demand at different levels. A utilization of the geothermal resource at 5000 full load hours corresponds to a split of geothermal:peak-supplier 90:10 for work and 50:50 for power. The corresponding values for 6000 full load hours are 80:20 for work and 35:65 for power.

Table 6 Reference case input data

Parameter	Dimension	Value	Parameter	Dimension	Value
Reservoir			Surface thermal water system		
Depth	M	1200–1400	Flowline length	m	200
Temperature	°C	75	Flowline inner diameter	m	0.23
Static reservoir pressure	MPa	15.4	Wall thickness	m	0.004
Water salinity	g l^{-1}	200	Insulation thickness	m	0.037
Gas content	Sm^3/m^3	0.25	Heat exchanger heat flux density	W m^{-2} K^{-1}	900
Methane content	Sm^3/Sm^3	0.88	Pinch point	K	4
Gas dissolution pressure	MPa	1.5	Material		CS, SS
Effective reservoir thickness	M	40	Injection pump motor efficiency	–	0.90
Permeability	m^2	0.18 10^{-12}	Injection pump isentropic efficiency	–	0.90
			Injection system efficiency	–	0.96
Wells: doublet with vertical production and deviated injection well			Total system: coupling with peak-load and redundancy-boiler		
Well depth	M	1400	Surface system operating pressure	MPa	1.5
Casing outside diameters	in	13 3/8, 9 5/8, 7	Correction factors output to design	–	1.1 to 1.2
Thermal conductivity casing	W m^{-1} K^{-1}	50	System availability	–	0.92
Thermal conductivities cement/rock	W m^{-1} K^{-1}	1.6/3			
Completion			Base case cost and revenue estimates		
Production pump	in	10.25	Thermal water mass flow rate	kg s^{-1}	42.5
Pump motor efficiency	–	0.85	Return temperature distribution grid	°C	35
Pump isentropic efficiency	–	0.78	Full load hours geothermal	h	6000
Production system efficiency (converter, transformer, power transm.)	–	0.9126	Power split geoth: peak load supplier	MW:MW	35:65
Pump minimum submergence	MPa	1.5	Work split Geoth: peak load supplier	GWh:GWh	80:20
Thermal conductivity tubing	W m^{-1} K^{-1}	50	Heat price at distribution grid	cents/kWh	8
Thermal conductivity annulus (gas)	W m^{-1} K^{-1}	0.035	Electricity purchase price	€/kWh	0.16
			Gas purchase price	€/kWh	0.04
			Lifetime	a	30

The modeling of the thermal water cycle was carried out for a reference case and sensitivities to evaluate the impact of variations in the controllable parameters on net present value and levelized cost. The data for the reference case are shown in Table 6. They are site-specific or were adopted from other geothermal projects (Schlagermann 2013, 2014; Kölbel et al. 2010).

The prognosis for the geothermal power in the reference case is 5.5 MW; the total power of the coupled total system is ca. 15.7 MW. The annual heat supply of the coupled system for the load structure in Fig. 5 amounts to approx. 41 GW p.a. corresponding to an annual cash-in of 3.3 million Euros p.a. for the total system at a heat price of 8 cents/kWh.

For the reference case, the cost model leads to an initial *capital expenditure* of approx. 14 million Euros, see Table 7. In addition, there is a further approx. 10 million Euro necessary for replacement investments over the operating period of 30 years. The model-implied annual operating expenditure is 1.63 million Euros.

The results for revenues, capital and operating expenditures lead to a *net present value* of 2.5 million Euros for the reference case over the operating period of 30 years, at a discount rate of 6%. The levelized cost of heat, defined as the ratio of the discounted capital and operating expenditures and the discounted heat work is 7.6 cents/kWh. For the determinations, expenditures and revenues were not inflated, and taxes were not considered.

Results

For a systemic optimization, the impact of the most important parameters on system work and power, net present value, and levelized cost of heat was investigated. These are full load hours, *FLH*, thermal water mass flow rate, *MaFl*, return temperature of the district heating network, *RLT*, heat price, electricity purchase price, *ElPr*, and financial support of well costs, *FoeS*. The results are shown in the following diagrams, Figs. 6, 7, and 8.

Table 7 Expenditures for the reference case

Initial capital expenditures, 10^3 Euro				
Planning	930	Data Acquisition = 500	Feasibility = 180	Consultations = 250
Wells	8114	Site = 453	Drilling = 6080	Evaluation = 1581
Production pump	632	Pump setting depth = 612 m	El. power = 332 kW	
Completion	141	Tubing, Power Cable = 99	Pump installation = 42	
Heat exchanger	894	Area = 1828 m^2	Geoth. power = 5.5 MW	Geoth. work = 32.90 GWh
Surface System	606	Piping, fittings, I&C = 536	Filters, pressure vessels = 70	
Injection pump	191	El. power = 336 kW		
Peak load boiler	1028	Power = 15.7 MW	Peak load work = 8.2 GWh	
Others	1501	Project management = 928	Public relations = 400	Power, data, insurances = 400
Total initial capital expenditure	14,037			
Euro Operating expenditures, 10^3 Euros p.a				
Energy-/resource-related	1006	Electricity = 641	Gas = 329	Other = 36
Human resources	489	Human resources = 234	Maintenance, Repair = 137	Other = 118
Other (insurance, and public relations)	137	Liability ins. = 90	Electronics, and machine breakdown ins. = 22	Other = 25
Total initial operating expenditure	1630			

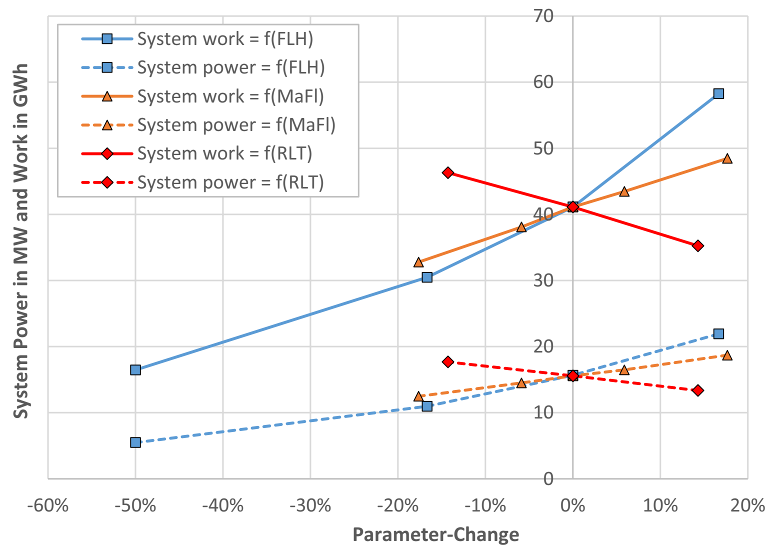

Fig. 6 Parameter dependency of system thermal power and work

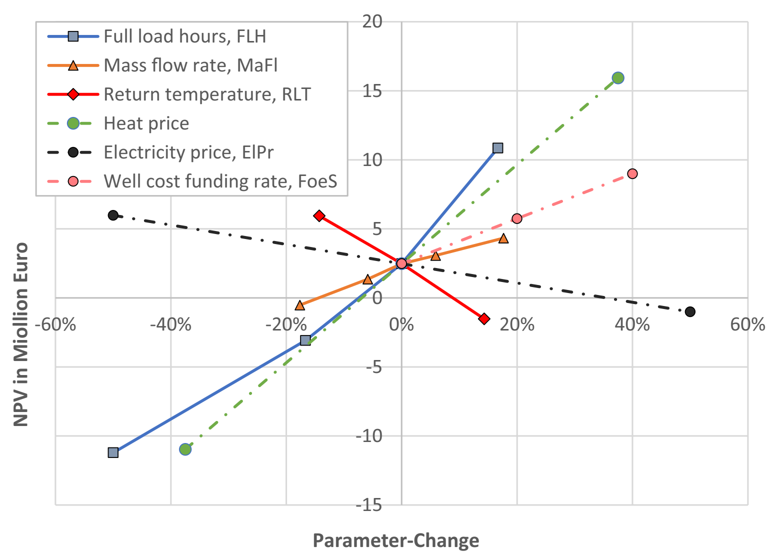

Fig. 7 Parameter dependency of net present value

Figure 6 shows the dependency of total system heat power and work as full load hours, mass flow rate and return temperature are changed. Of the three parameters, the geothermal full load hours have by far the highest impact on the thermal output, followed by thermal mass flow rate and return temperature. The minus 50% change in full load hours from the reference state of 6000 to 3000 load hours leads to a geothermal system without coupling, i.e., a system supplying approx. 16.5 GWh heat at a power of 5.5 MW.

Figure 7 shows the impact of changes in the foregoing parameters on net present value, in addition to variations in heat price, purchase price for electricity, and well cost funding rate. As depicted, the case without a peak supplier is not economically viable at

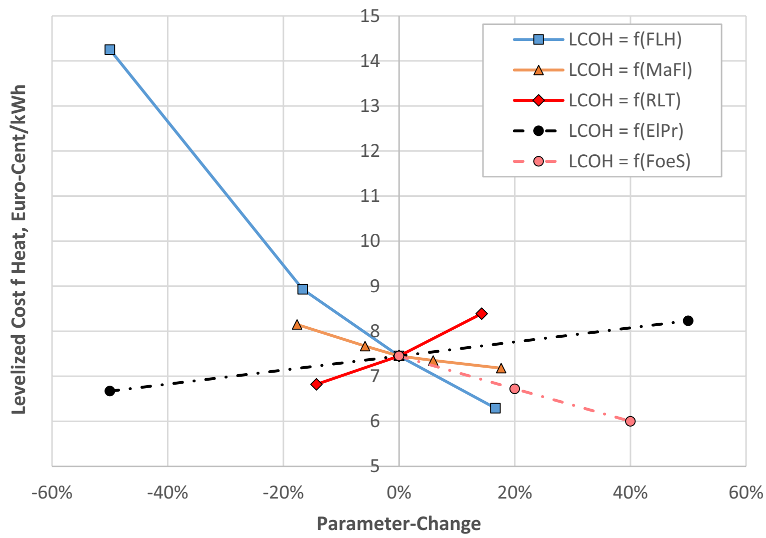

Fig. 8 Parameter dependency of levelized cost of heat

8 cents/kWh and zero funding rate. To break even, a 40% drilling expenditure funding and a heat price of around 12 cents/kWh would be required.

Figure 8 shows the impact of changes in full load hours, mass flow rate, return temperature, electricity price, and well cost funding on the levelized cost of heat. With more than 14 cents/kWh LCOH at the transfer point into the district heating network the case without a peak supplier is significantly above the cost of coupled systems, with geothermal energy supplying heat at base load.

The aforementioned results represent the success case. As shown in Reinicke et al. (2022), Hollmann et al. (2023), geological risks can be included in such an analysis and a monetary expected value can be determined that incorporates these risks. The scenario-based calculation of the monetary expected value (EMV) supports project selection from a portfolio, but more importantly, it supports the identification and quantification of the critical factors for the success of a project.

Discussion

The presented procedure provides a comprehensible means to evaluate deep geothermal projects. Determined net present value and levelized cost provide profitability indicators, which may also be used to rank projects and manage portfolios of heat supply opportunities.

In its approach the methodology is very similar to the work documented in Mijnlieff et al. (2012), Wees et al. (2012). Mijnlieff et al. and van Wees et al. provide a probabilistic fast model for performance assessment of geothermal doublets for direct heat applications. For the thermodynamics of the thermal cycle this contribution provides a more detailed description of the cycle and relies on the Reference Fluid Thermodynamic and Transport Properties Database of the National Institute of Standards and Technology NIST, Refprop (Lemmon et al. 2018), to evaluate fluid properties and their subsequent correction for salinity. Despite these differences, agreement between both model results is quite good, see Table 3. For the economic evaluation, models to size and cost components are provided and calibrated using information from real-life endeavors. The coupling of geothermal to other heat generation systems allows a systemic optimization of serving a market of defined demand structure.

The application of the procedure to the geologic setting in the Hannover–Celle area shows that geothermal projects are economically viable to supply district heating networks, if they are allowed to deliver the heat at baseload, with a coupled system serving as peak load supplier.

The results presented for the reference case are dependent in particular on full load hours, heat sales price, and return temperature.

As shown in Figs. 6, 7, and 8, *full load hours* are the most critical parameter for the economic success of a deep geothermal heat project. Thus, every effort should be made, to couple a geothermal system with a peak load supplier. To achieve the 6000 load hours p.a. in the reference case, a gas-fired boiler was assumed for peak load supply designed in such a way that it can also serve as backup of the geothermal system. At the assumed load hours, the gas-fired boiler would supply 20% of the heat, at 5.000 load hours its contribution would be only 10% of sales. The costs of the boiler are included in the economic calculations. A price of 4 cents per kWh was assumed for gas purchase costs. This gas price is higher than the average spot prices during the past decade but lower than the current price.

There are other ways for peak load coverage, such as the use of biogas, hydrogen, or a seasonal storage of heat in the summer months. A seasonable storage, using surplus energy of wind and power in the summer, would increase the original reservoir temperature and thus lead to an increased heat supply in the winter months. Such a seasonal storage is investigated within the research project GeoTES (Clausthal and Celle 2022), but is not subject of this work.

Although the assumed *heat price* at the transfer point into the district heating network is significantly lower than the levelized costs of near-surface geothermal systems with heat pumps, which range from 15 to 25 cents per kWh and more, depending on type, size and location, it is higher than past district heating prices at the end consumer, which include distribution. The end consumer price for district heat was capped at 9.5 cents per kilowatt-hour for customers by the federal government end 2022 (Bundesministerium der Justiz 2022). Full cost covering prices for heat are expected to be higher than this cap in the future.

Return temperatures of 35 degrees Celsius are unusual in conventional heating networks. They can be achieved by cascading utilization with low-temperature consumers at the end or using large scale heat pumps. The use of heat pumps was not considered in the economic calculations.

To increase *thermal mass flow rate* as a further parameter of importance for economic success, the options provided by directional drilling and stimulation technology should be investigated. These means have the potential to significantly increase the flow rate of the thermal cycle.

Self-generation of electric power to supply in particular the pumps may be an opportunity to improve economics.

A sufficiently large *heat market* in the vicinity, able to absorb the produced heat, is as important as the technical and economic requirements above.

Conclusion

The presented procedure and its computational implementation in MATLAB allow a rigorous evaluation of deep geothermal projects by a reasonable effort even for scenario variations. Calculated net present values and levelized cost allow an assessment of economic viability, and comparisons with other competing assets or other sources of heat supply. The results presented for variations of the controllable parameters may be used in systemic optimizations.

The thermodynamic part of the procedure leads to a reliable estimate for the recoverable heat verified by comparing the results with an actual geothermal project. The cost model of the economic part of the procedure has been validated with biding results and cost information from actual projects and modified as appropriate. The significant price increases in well and component cost, experienced recently for various reasons, are not reflected in the cost model.

Applying the procedure, using subsurface and surface conditions in the Hannover–Celle area as an example, shows that geothermal projects are economically viable to supply heat. Precondition is they can be used to supply baseload heat with a coupled system for peak load supply. The full load hours of the geothermal part of the coupled system are the most critical parameter for an economic success. Other options to improve the economics, worth investigation, are increasing mass flow rate and decreasing return temperature and the self-generation of electric power.

Abbreviations

List of symbols

A	Area, m^2
c	Compressibility, Pa^{-1}
c_p	Isobaric (mass) heat capacity, $kJ\ kg^{-1}\ K^{-1} = kWs\ kg^{-1}\ K^{-1}$
Capex	Capital expenditure (initial or replacement), €
d	Diameter, m
EMV	Expected monetary value, €
FLH	Full load hours, h
g	Acceleration of gravity, $m\ s^{-2}$
h	Enthalpy, $kJ\ kg^{-1}$
h	Thickness, height, m
k	Permeability, m^2
k	Coefficient of heat transfer, $W\ m^{-2}\ K^{-1}$
L	Length, m
LCOH	Levelized cost of heat, Cent/kWh
$\dot{m}$	Mass flow, $kg\ s^{-1}$
n	Project lifetime, a
NPF	Name plate factor, –
NPV	Net present value, €
Nu	Nußelt number, –
Opex	Operating expenditure, €
p, Δp	Pressure, pressure difference, MPa
p_i	(Undisturbed) initial reservoir pressure, MPa
POS	Probability of success, –
Pr	Energy price, €/kWh
P	Power, kW
P_{hydr}	Hydraulic power, kW
P_{gt}	Geothermal power, kW
P_{coup}	Coupled power, kW
Pr	Prandtl number, –
q_w	Heat flux density, $W\ m^{-2}\ K^{-1}$
r	Radial distance from well center, m
R	Thermal resistance, $K\ W^{-1}$
Re	Reynold's number, –
S	Storage coefficient, –
t	Time since start of production/injection, s

T_{GW}	Transmissivity, $m^2\ s^{-1}$
T_i/T_o	Flow/return temperature, inflow/outflow temperature, K
T_0	Temperature of the environment, undisturbed formation temperature, K
U	(Flow conduit) circumference, m
v	Flow velocity, $m\ s^{-1}$
V	Volume, m^3
$\dot{V}$	Volumetric flow rate, $m^3\ s^{-1}$
Z	Discount rate, –
z	Depth, elevation, m

Greek symbols

α_{Brine}	Convective heat transfer coefficient, $W\ m^{-2}\ K^{-1}$
α	Pressure factor, –
ε	(Pipe inside) roughness, m
η	Efficiency, –
λ	Coefficient of friction, –
λ	Heat conductivity, $W\ m^{-1}\ K^{-1}$
μ	Dynamic viscosity, Pa s
φ	Porosity of the reservoir rock, –
ρ	Density, $kg\ m^{-3}$

Acknowledgements
The work is based on the dissertation "Exergoökonomische Analyse geothermischer Strombereitstellung am Beispiel des Oberrheingrabens" by Pascal Schlagermann, Technische Universität München, Lehrstuhl für Energiesysteme. Prof. Dr. Peter Reichetseder and Dipl. Ing. Dieter Rudschinski gave valuable support in preparing the manuscript.

Author contributions
PS: thermodynamic and economic model and MATLAB Code; KMR: subsurface data, model modification, model application, preparation of manuscript.

Funding
Open Access funding enabled and organized by Projekt DEAL. Open Access funding is enabled and organized by Projekt DEAL.

Availability of data and materials
Further information on the data sets used, analyzed or generated during the current study are available from the corresponding author on a reasonable request.

Declarations

Competing interests
There is no competing interest to disclose.

Received: 20 June 2023 Accepted: 7 November 2023
Published online: 21 November 2023

References

Beggs H, Brill J. A study of two-phase flow in inclined pipes. J Pet Techn. 1973;25:607–17.
Beitz W, Grote K-H. Taschenbuch für den Maschinenbau / Dubbel (20 Auflage). Heidelberg: Springer; 2001.
Blank L, Rioseco EM, Caiazzo A, Wilbrandt U. Modeling, simulation, and optimization of geothermal energy production from hot sedimentary aquifers. Comput Geosci. 2021;25:67–104.
Bohl W, Elmendorf W. Technische Strömungslehre (13 Auflage). Würzburg: Vogel Buchverlag; 2005.
Bundesministerium der Justiz. EWPBG, Gesetz zur Einführung von Preisbremsen für leitungsgebundenes Erdgas und Wärme (Erdgas-Wärme-Preisbremsengesetz – EWPBG); 2022. EWPBG - Gesetz zur Einführung von Preisbremsen für leitungsgebundenes Erdgas und Wärme (gesetze-im-internet.de). Zugriff am 10 Feb 2023.
Clausthal TU, Drilling Simulator Celle. GeoTES: Möglichkeiten und Grenzen thermischer Energiespeicherung in tiefen Aquiferen (Georeservoiren) im Rahmen der "Wärmewende 2030"; 2022. https://www.ite.tu-clausthal.de/en/research/geothermal-systems/projects/current-projects/geotes. Zugriff am 10 Feb 2023.
ETHZ. genGEO. ETH Zürich; 2020. https://github.com/GEG-ETHZ/genGEO. Zugriff am 09 June 2023.
Fromme J. Räumliche Implikationen von Regenerativ-Energieszenarien für die langfristige Entwicklung des deutschen Stromversorgungssystems. Dortmund: Universität Dortmund, Fakultät für Raumplanung; 2005.
Guth A. Monte-Carlo-Simulation der Stromgestehungskosten für Geothermie im Oberrheingraben. Karlsruhe: Karlsruher Institut für Technologie, Lehrstuhl für Energiewirtschaft; 2011.
Herzberger P, Schlagermann P, Heyder B, Münch W. Geothermiekraftwerk Bruchsal—Strom aus dem Rheingraben. VBI Beratende Ingenieure. 5; 2009.
Hollmann G, Reinicke K, Reichetseder P. Probabilistic risk and value assessment transferred from E&P to geothermal applications. In: EAGE annual 84th conference & exhibition, 5–8 June 2023. https://doi.org/10.3997/2214-4609.202310392, Vienna Austria; 2023.

Kalb J, Steinhilber T. Skriptum zur Vorlesung Wärmetransportphänomene. Lehrstuhl für Thermodynamik, Technische Universität München; 2003.
Kölbel T, Schlagermann P, Münch W, Zorn R, Rettenmaier D. Geothermiekraftwerk Bruchsal - Erste Messergebnisse. bbr Fachmagzin für Brunnen - und Leitungsbau. bbr Fachmagzin für Brunnen - und Leitungsbau, Nr. Sonderheft, pp. 2–7; 2010.
Lemmon EW, Bell IH, Huber ML, NcLinden MO. NIST Standard reference database 23: reference fluid thermodynamic and transport properties-REFPROP, Version 10.0. NTIS, National Institute of Standards and Technology, Standard Reference Data Program, Gaithersburg; 2018. https://doi.org/10.18434/T4/1502528. Zugriff am 27 Nov 2022.
Mijnlieff HF, Obdam AN, Van Wees JD, Pluymaekers MP, Veldkamp JG. TNO report: doubletCalc 1.4 manual, TNO 2012 R11396. Utrecht: TNO; 2014.
NREL. NREL/GEOPHIRES v2.0. National Renewable Energy Laboratory; 2018. https://github.com/NREL/GEOPHIRES-v2. Zugriff am 09 June 2023.
Ozbek H, Phillips SL. Thermal conductivity of aqueous sodium chloride solutions from 20 to 330 °C. J Chem Eng Data. 1980;3(25):263–7.
Pitzer KS, Peiper JC, Busey RH. Thermodynamic properties of aqueous sodium chloride solutions. J Phys Chem Ref Data. 1984;13:1–102.
Reinicke KM, Hollmann G, Reichetseder P. Probabilistische Risiko- und Wirtschaftlichkeitsbewertung von Geothermieprojekten. Erdöl Erdas Kohle, EEK. p. 35–44. 138 Jg.Ausgabe 11; 2022.
Rose & Associates. Statistics: the language of uncertainty probabilities and distributions—2, LLP, Ch 2—statistics, 5D RA V 2007–02.1. Houston: Rose & Associates; 2007.
Sanchez E, Torres CF, Guillenc P, Larrazabal G. Modeling and simulation of the production process of electrical energy in a geothermal power plant. Math Comput Model. 2013;57:2140–8.
Schlagermann P. Förderpumpenperformance im Geothermieprojekt Bruchsal. In: Geothermie workshop, EnBW Energie Baden-Württemberg AG; 2013.
Schlagermann P. Dissertation: Exergoökonomische Analyse geothermischer Strombereitstellung am Beispiel des Oberrheingrabens. München: Technische Universität München, Lehrstuhl für Energiesysteme; 2014.
Shamoushaki M, Manfrida G, Talluri L, Niknam PH, Fiaschi D. Different geothermal power cycle configurations cost estimation models. Sustainability. 2021;13(11133):1–19.
Shide M, Zhenhao D. The viscosity of aqueous alkali-chloride solutions up to high temperature, pressure and ionic strength. J Chem Eng Data. 2008;30:1510–23.
Sperber A, Uhlig S, Matthiasson M. Verrohrungsschemata und Casingdesign für tiefe GT-Bohrungen – ausgewählte Fallbeispiele. In: Der Geothermiekongress (pp. 170–180), Geothermische Vereinigung—Bundesverband Geothermie e.V., Karlsruhe; 2008.
Tischner T, Krug S (Editoren). GeneSys: test- und Erschließungsarbeiten im Zeitraum 2010–2011 Interne Dokumentation der Arbeiten an der Geothermiebohrung Groß Buchholz Gt1. Hannover: Bundesanstalt für Geowissenschaften und Rohstoffe (BGR) & Leibniz-Institut für Angewandte Geophysik (LIAG); 2012.
Turton R, Bailie R, Whiting WB, Shaeiwitz JA, Bhattacharyya D. Analysis, synthesis and design of chemical processes. Upper Saddle River: Prentice Hall; 2009.
Umweltbundesamt. Kommunaler Klimaschutz durch Verbesserung der Effizienz in der Fernwärmeversorgung mittels Nutzung von Niedertemperaturwärmequellen am Beispiel tiefengeothermischer Ressourcen. BM für Umwelt, Naturschutz und nukleare Sicherheit, Umweltforschungsplan, 3715 41 112 0 FB000442, Dessau-Roßlau; 2018.
van Wees J-D, Kronimus A, van Putten M, Pluymaekers MP, Mijnlieff H, van Hooff P, Obdam A, Kramers L. Geothermal aquifer performance assessment for direct heat production—methodology and application to Rotliegend aquifers. Netherlands J Geosci Geologie En Mijnbouw. 2012;91(4):651–65.
VDI. Wirtschaftlichkeit gebäudetechnischer Anlagen, Grundlagen und Kostenberechnung. Düsseldorf: Verein deutscher Ingenieure; 2010.
Wagner W. Wärmeübertragung. 6th ed. Würzburg: Vogel Buchverlag; 2004.
Walzebuck JP, Gaupp R. Zur Temperaturgeschichte des Gasfeldes Thönse. In: Das Gasfeld Thönse—Ein Unikat. Hannover: Niedersächsische Akademie der Geowissenschaften; 1991. p. 132–6.
Wikipedia. Wikipedia; 2023. https://en.wikipedia.org/wiki/Levelized_cost_of_electricity. Zugriff am 25 Mar 2023.
Zanke U. Zur Berechnung von Strömungs-Widerstandsbeiwerten. Wasser Und Boden. 1993;45(1):14.

Publisher's Note